JOURNAL OF Materials CHEMISTRY

Tilt-polarization coupling in a homologous series of ferroelectric liquid crystals

Jochen Schacht,* Heike Baethge, Frank Giesselmann and Peter Zugenmaier

Institut für Physikalische Chemie, Technische Universität Clausthal, Arnold-Sommerfeld-Straße 4, D-38678 Clausthal-Zellerfeld, Germany

The synthesis of the homologous series 4-[(*S*)-2-chloro-4-methylpentanoyloxy]-4′-[4-alkylbenzoyloxy]biphenyl and their chiral and mesomorphic properties are reported. The enantiomeric excess is deduced from ^{1}H NMR spectroscopy. For the hexyl derivative, a twist grain boundary state (TGB_A*) mediates the cholesteric to SmC* phase transition and its stability is discussed in terms of chirality and surface interactions. In the SmC* phase, measurements of the spontaneous polarization are reported and the temperature dependence of the tilt angle is determined from the electro-optical switching process or deduced from X-ray measurements of the smectic layer thickness, respectively. The tilt-polarization coupling is discussed within the framework of the 'generalized Landau model' proposed by Žekš and Blinc.

Chiral α-chloro acids derived from natural amino acids[1,2] are successfully used in the synthesis of ferroelectric liquid crystals with high spontaneous polarization.[3–7] Over a broad temperature range, the SmC* phase is formed in some benzoate derivatives.[5,8,9] In general, these materials exhibit a rich mesomorphism including N*, SmA*, SmC* and higher ordered smectic phases.[10–11] Frustrated liquid crystalline phases, like blue phases[7,11] or twist grain boundary phases,[12–16] occur in some of these materials. We have modified the molecular structure of ferroelectric liquid crystalline materials of the type mentioned above to increase the number of enantiotropic tilted smectic phases which are particularly attractive for investigations of their structure and dynamical properties. Furthermore, phase transitions like N*→SmA*, N*→SmC*, SmA*→SmC* or SmC*→tilted hexatic phases can be studied in detail.[17]

In this paper we report the synthesis of the homologous series **S1B*n*** with their general chemical formula as shown.

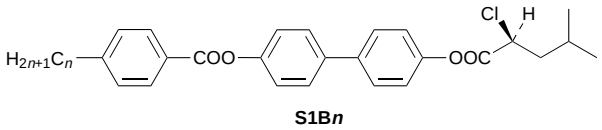

S1B*n*

N*, SmA*, TGB_A*, SmC* and higher ordered smectic phases were characterized by texture observations, DSC, electro-optical measurements and by X-ray scattering techniques. The absolute enantiomeric excess of these compounds was deduced from ^{1}H NMR spectroscopy. The results are discussed with respect to chiral properties, as spontaneous polarization or stability of the TGB_A* state. Temperature dependent tilt angle measurements obtained from the ferroelectric switching process and from X-ray scattering data are reported as well as tilt-polarization coupling which is discussed in the framework of the 'generalized Landau theory' proposed by Žekš and Blinc.[18,19]

Experimental

Compounds **S1B*n*** were synthesized according to a straightforward three step procedure depicted in Scheme 1. (*S*)-2-Chloro-4-methylpentanoic acid **1** was derived from optically pure commercially available L-leucine. Starting from 4,4′-dihydroxybiphenyl, 4-[(*S*)-2-chloro-4-methylpentanoyloxy]-4′-hydroxybiphenyl **2** was prepared *via* esterification using the dicyclohexylcarbodiimide (DCC)/dimethylaminopyridine (DMAP) system or *via* the corresponding acyl chloride, respectively. Esterification of **2** with 4-*n*-alkylbenzoic acids leads to the target molecules **S1B*n***. Reaction conditions and spectroscopic data of the compounds are summarized in the Synthesis section.

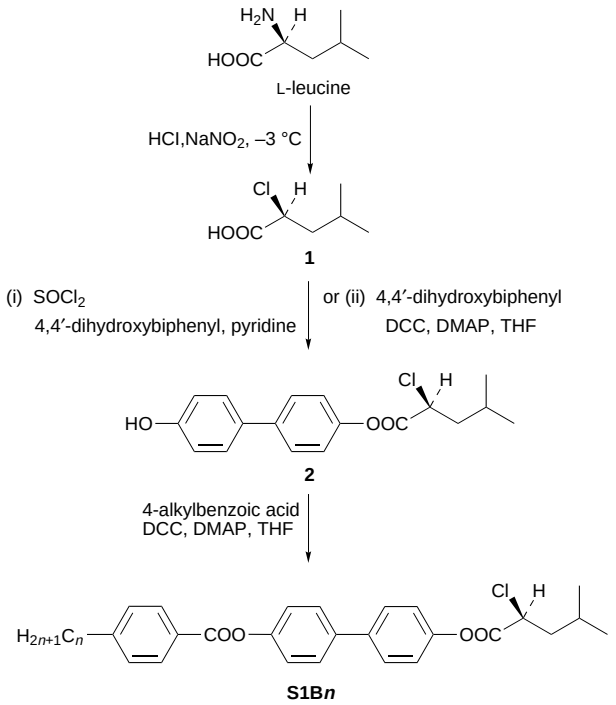

Scheme 1 Synthesis of compounds **S1B*n***

Calorimetric studies were carried out using a differential scanning calorimeter (Perkin Elmer DSC 7). Texture analyses were performed with a polarizing microscope, Olympus BH-2, equipped with a Mettler FP-52 hot stage connected to a Mettler FP-5 temperature controlling unit. The accuracy of the relative temperature lies within 0.1 K, the absolute temperature calibration within ±1 K. The materials were prepared between two untreated glass plates or in commercially available LC cells (E.H.C. Co. Ltd. Tokyo, polyimide coated, parallel

* E-mail: schacht@pc.tu-clausthal.de

rubbed, 4 μm cell gap) for texture observation; in addition, textures of uncovered droplets and free-standing films were studied.

The temperature dependence of the spontaneous polarization was investigated by the triangle wave method.[20] An electric field with a frequency of 210 Hz and an amplitude of 2 MV m^{-1} was used to achieve saturated switching in the SmC* phase. Ionic impurities do not affect the polarization reversal current at this high frequency, but, due to the low viscosity of materials, saturated ferroelectric switching occurs up to 2.5 kHz (2 MV m^{-1}). At one fixed temperature sixteen oscilloscope traces were averaged to reduce statistical noise.

The temperature dependence of the optical tilt angle Θ_{opt} was determined by an electrooptical switching experiment introduced by Bahr and Heppke.[21] In surface stabilized ferroelectric liquid crystals (SSFLC) geometry a square wave electric field (200 Hz, 2 MV m^{-1}) causes ferroelectric switching and the transmission of both polarization states $T_{up} \propto \sin^2[2(\phi - \Theta_{opt})]$ and $T_{down} \propto \sin^2[2(\phi + \Theta_{opt})]$ was recorded at a wavelength of 514 nm. ϕ denotes the angle between the polarization direction of the polarizer and the direction of the smectic layer normal which defines the position of a domain between crossed polarizers. A photomultiplier detected the transmission curves T_{up} and T_{down} as a function of ϕ when rotating the sample with respect to the plane of polarized light. The measured transmission curves were fitted to the functions T_{up} and T_{down}. The phase shift between both curves is twice the optical tilt angle Θ_{opt}.

Using a Kratky small angle camera (Anton Paar KG), the temperature dependence of the smectic layer spacing was determined from X-ray scattering data recorded with a one dimensional detector (Firma M. Braun). Standard crystalline materials were used for calibration. The tilt angle $\Theta_{X\text{-}ray}(T)$ was determined by the ratio of the smectic layer thickness found in the SmC* phase $d_{SmC*}(T)$ and the spacing in the SmA* phase d_{SmA*} according to eqn. (*a*).

$$\Theta_{X\text{-}ray}(T) = \arccos \frac{d_{SmC*}(T)}{d_{SmA*}}. \qquad (a)$$

^{1}H NMR spectra were used to elucidate the enantiomeric excess. They were obtained on a Bruker ARX (400 MHz) spectrometer with tetramethylsilane (TMS) as internal standard and deuterochloroform ($CDCl_3$) as solvent. Mass spectra were obtained on a HP 4989B mass spectrometer (70 eV, direct injection probe).

Results and Discussion

Polarizing microscopy and DSC measurements

In general, the homologous series **S1B*n*** shows cholesteric, SmA* and tilted smectic phases. Phase transition temperatures and transition enthalpies are summarized in Table 1, and the range of stability of phases is shown in Fig. 1. Within a small temperature range compound **S1B2** possesses a monotropic cholesteric phase. An extension of the alkyl chain length by one methylene unit leads to the formation of an enantiotropic cholesteric phase in compound **S1B3**, which in addition possesses a monotropic SmC* phase. Further elongation of the terminal alkyl chain stabilizes the SmC* phase. An enantiotropic SmA* phase is inserted between N* and SmC* phases for homologues **S1B*n*** with $n \geqslant 6$. A hexatic tilted smectic phase (SmX_1*) is located in a temperature range below the SmC* phase of **S1B*n*** with $n \geqslant 5$. It is evident from a comparison of DSC traces in a heating–cooling cycle (*cf.* Fig. 2 and 3) that the SmX_1* phase is monotropic in compounds **S1B5**, **6** but enantiotropic in homologues **S1B7**, **8**. Compounds **S1B*n*** with $6 \leqslant n \leqslant 8$ form a second monotropic higher ordered smectic phase, SmX_2*, as can be concluded from DSC cooling traces (*cf.* Fig. 3).

In compounds **S1B6**, **7**, **8** a distinct peak appears at the SmA*→SmC* phase transition, clearly developed in the DSC traces of compound **S1B6**. The phase transition is classified as first order with phase transition enthalpies between 200 and 600 J mol^{-1}, which are comparable to molar enthalpy differences $\Delta\bar{H}$ for a N*→I phase transition (200–1000 J mol^{-1}). Compound **S1B6** undergoes a transition from the SmA* to N* phase (and *vice versa*) by way of an intermediate twist grain boundary state (TGB_A*). The SmA*→TGB_A*→N* phase sequence appears as a step in DSC heating and cooling traces, whereas thermograms of **S1B7**, **8** indicate a peak associated with a SmA*→N* phase transition accompanied by a $\Delta\bar{H}$ comparable to values found for the N*→I phase transition. Results of a detailed calorimetric study performed in the vicinity of the SmA*→TGB_A*→N* phase sequence in compound **S1B6** are discussed below with respect to different heating–cooling rates and variable sample masses.

Fig. 4–7 depict typical textures of mesomorphic phases of homologues **S1B*n*** observed by polarizing microscopy and serve to identify several of the phases obtained.[22] The polygonal texture of the cholesteric phase of compound **S1B7** is depicted in Fig. 4(*a*) at a temperature of 1 K above the SmA*→N* phase transition. The disclination lines, due to the cholesteric helix, are clearly visible. In compound **S1B6**, the cholesteric fan shaped texture is depicted in Fig. 4(*b*) (lower part) together with the Grandjean texture with typical 'oily streaks' of the cholesteric phase (upper part). Fig. 4(*c*) depicts the filament texture of the TGB_A* state, which mediates the phase transition between the SmA* and N* phases in compound **S1B6**.

At the edge of an uncovered droplet (**S1B6**) depicted in Fig. 5(*a*), smectic layers are oriented parallel to the substrate (homeotropic alignment) and edge disclination lines occur in the helical SmC* phase. Their origin resembles that of the Gandjean–Cano pattern of edge dislocations in a cholesteric wedge.[23] These lines vanish after heating the sample into the nonhelical SmA* phase [*cf.* Fig. 5(*b*)], where the homeotropic part of the droplet appears dark between crossed polarizers. In a heating process, some characteristic filaments of the intermediate TGB_A* state are growing from the middle of the droplet towards the surface area [*cf.* Fig. 5(*c*)] just before the cholesteric phase is formed.

On heating a free standing film (**S1B6**), the TGB_A* filament texture grows from the meniscus of the film into the middle. If the film thickness falls short of a critical value, an SmA* phase [lower right dark area of Fig. 6(*a*)] is formed instead. In agreement with results of Dierking *et al.*,[24] the TGB_A* state is suppressed in confined geometry. On cooling the free standing film, typical platelet textures of the smectic SmX_1* [*cf.* Fig. 6(*b*)] and the SmX_2* phase [*cf.* Fig. 6(*c*)] are obtained.

Mechanical shearing in the SmC* phase of compound **S1B7** prepared between two untreated glass plates leads to homeotropic alignment of smectic layers as can be seen from the typical Schlieren texture depicted in Fig. 7(*a*). This texture changes color and shape slightly after cooling the sample into the SmX_1* phase which maintains the Schlieren texture [*cf.* Fig. 7(*b*)]. After cooling the sample to the SmX_2* phase, this Schlieren texture is more significantly altered [*cf.* Fig. 7(*c*)]. Recently performed experiments indicate that SmX_1* resembles the SmI* phase and SmX_2* is similar to an SmF* phase, respectively. This is concluded from saturated ferroelectric switching being present in both higher ordered phases up to 10 K below the SmX_1*→SmX_2* phase transition temperature. Their hexatic nature is unambiguously established by X-ray wide angle scattering patterns recorded using freely suspended films oriented in an electric field.[25]

DSC measurements in the vicinity of the SmA*→TGB_A*→N* phase sequence

A significant change in the molar heat capacity is associated with the SmA*→TGB_A*→N* phase sequence in a small

Table 1 Phase transition temperatures (°C) in the homologous series **S1B*n*** with ee = 60%. Enantiotropic phases are marked with ●, whereas ○ denotes monotropic phases. Compound **S1B6** undergoes a phase transition from the cholesteric phase into the SmA* phase (and *vice versa*) by an intermediate TGB_A* state. Values of $\Delta\bar{H}$/J mol^{-1} of the phase transitions are printed in *italics*

	homologous series **S1B*n***													
n	K		SmX_2*		SmX_1*		SmC*		SmA*		TGB_A*		N*		I
2	●	117											○	115	●
		28600												*184*	
3	●	83					○	67					●	103	●
		20600						*230*						*350*	
5	●	77			○	71	●	107	●				●	124	●
		14300				*1760*		*270*						*640*	
6	●	80	○	69	○	75	●	116	●	120	●	120.1	●	130	●
		15100		*270*		*1620*		*550*						*780*	
7	●	64	○	63	●	73	●	117	●	130			●	137	●
		13000		*100*		*1900*		*220*		*360*				*860*	
8	●	62	○	60	●	75	●	119	●	131			●	136	●
		11700		*70*		*2220*		*270*		*850*				*950*	

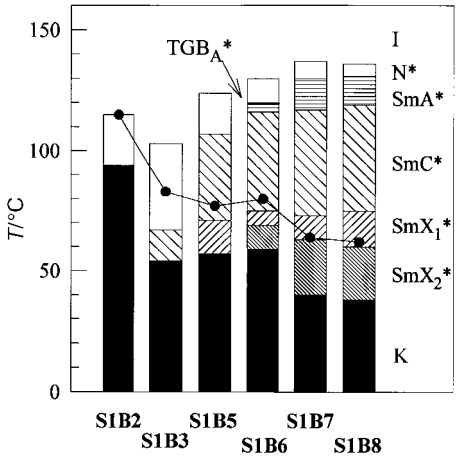

Fig. 1 Temperature range of stability of mesomorphic phases in the homologous series **S1B*n***. Monotropic phases are shown below the solid line representing the melting temperature of the crystalline phase.

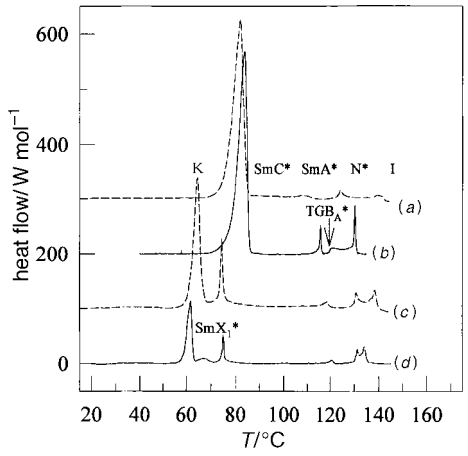

Fig. 2 DSC traces for heating cycles (rate: 5 K min^{-1}), (*a*) **S1B5**, (*b*) **S1B6**, (*c*) **S1B7**, (*d*) **S1B8**

amount of **S1B6** (0.92 mg) irrespective of the heating–cooling rate as can be concluded from a comparison of DSC traces depicted in Fig. 8(*a*), (*b*). Neither the shape of the DSC traces nor $\Delta\overline{c_p}$ values are significantly altered by an increase of the sample mass accompanied by a reduction of the sample's surface to volume ratio [*cf.* Fig. 8(*c*), (*d*)]. Therefore, surface effects are considered to be less important in these samples, and bulk properties are detected. A mean value of $|\Delta\overline{c_p}| = 135 \pm 7$ J K^{-1} mol^{-1} is found. Since a pure twist deformation of the spatial director configuration is incompatible with the

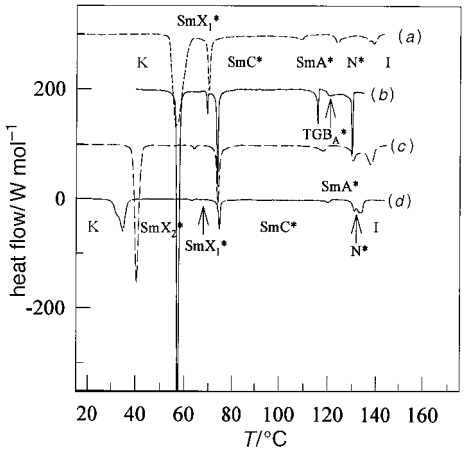

Fig. 3 DSC traces for cooling cycles (rate: −5 K min^{-1}); (*a*) **S1B5**, (*b*) **S1B6**, (*c*) **S1B7**, (*d*) **S1B8**

layered structure of a non-tilted smectic phase, the TGB_A* state can mediate the transition between the cholesteric and the SmA* phase in such a manner that the SmA* phase adopts the twist of the cholesteric phase by creation of a lattice of screw dislocations (grain boundaries). The overall phase transition therefore becomes continuous, which might explain the shape of the DSC curves. A similar shape for DSC traces has been reported by Werth *et al.*[26] and Navailles *et al.*[15] for compounds with a SmA*→TGB_A*→N* phase sequence.

It can be concluded that a TGB_A* state is formed, if the 'twisting power' is high enough or if the smectic layer structure is destabilized. Therefore, the homologue **S1B6** with the least extended range of stability of the SmA* phase (smaller than 10 K) forms the TGB_A* state. The existence of a TGB_A* state demands molecular chirality.

Enantiomeric excess

Chiral properties of macroscopic phases, *e.g.* pitch of N* or SmC* phase, are related to molecular chirality. Both pure enantiomers exhibit effects of the same magnitude but of opposite sign. Hence, they vanish in the corresponding racemate. Results of detailed mixing studies of enantiomers establish a linear dependency of the spontaneous polarization on the enantiomeric excess (ee).[27] A discussion of results of simulations or molecular modelling procedures with respect to the influence of molecular chirality requires an exact determination of the absolute value of the ee.

(*S*)-2-Chloro-4-methylpentanoic acid **1** is derived from L-leucine in a double inversion process, which causes partial racemization. According to Scheme 2, esterification of **1** with

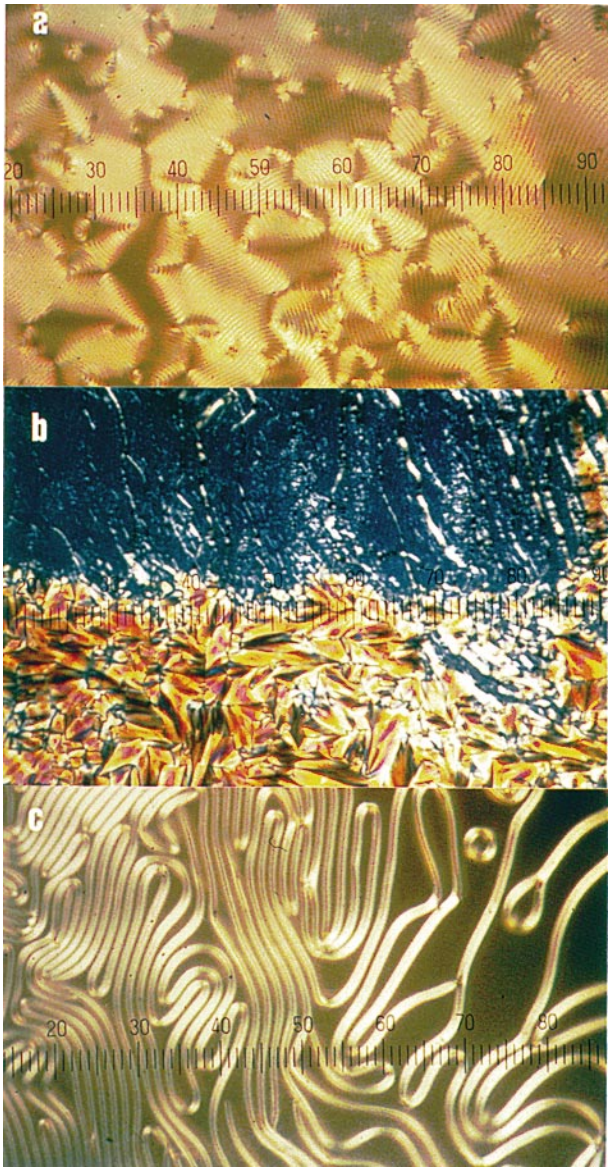

Fig. 4 Typical textures in the homologous series **S1B*n***: (a) polygonal texture of the cholesteric phase **S1B7**, (b) fan shaped texture and Grandjean texture of the cholesteric phase **S1B6**, (c) filament texture of the TGB_A* state **S1B6**; ten units of scale = 70 μm

optically pure (*R*)-2,2,2-trifluoro-1-(9-anthryl)ethanol affords a mixture of diastereomers **3*RS*** and **3*RR***, respectively. Substitution of the (*R*)-ethanol derivative by its mirror image leads to a mixture of diastereomers **3*SS*** and **3*SR***. Based on the assumption that the esterification step does not reduce the enantiomeric excess of **1**, the ee is determined by the ratios of diastereomers **3*RS*/3*RR***, and **3*SS*/3*SR***, respectively, which should be equal, if chiral differentiation of the alcohol derivatives in the esterification steps is negligible. In one of these mixtures, *e.g.* **3*SS*/3*SR***† (upper spectrum depicted in Fig. 9), each of the two CH_3 groups of each diastereomer appears as a doublet in the ^1H NMR (400 MHz, $CDCl_3$) spectrum. Altogether 2×2 doublets with a normalized integral intensity equal to six protons are located in a range of chemical shift δ between 0.72 and 0.88. Two doublets are located at δ 0.76, one of which (at lower δ) is related to **3*SS*** and the other appearing as a shoulder at larger δ is related to **3*RS***. Their signals are overlapped by the third doublet related to **3*RS*** at δ 0.785, whereas the fourth doublet (**3*SS***) is clearly separated at δ

† Enantiomers like **3*RS***, **3*SR*** are indistinguishable by ^1H NMR in $CDCl_3$. The same holds for a mixture of **3*RR***, **3*SS***.

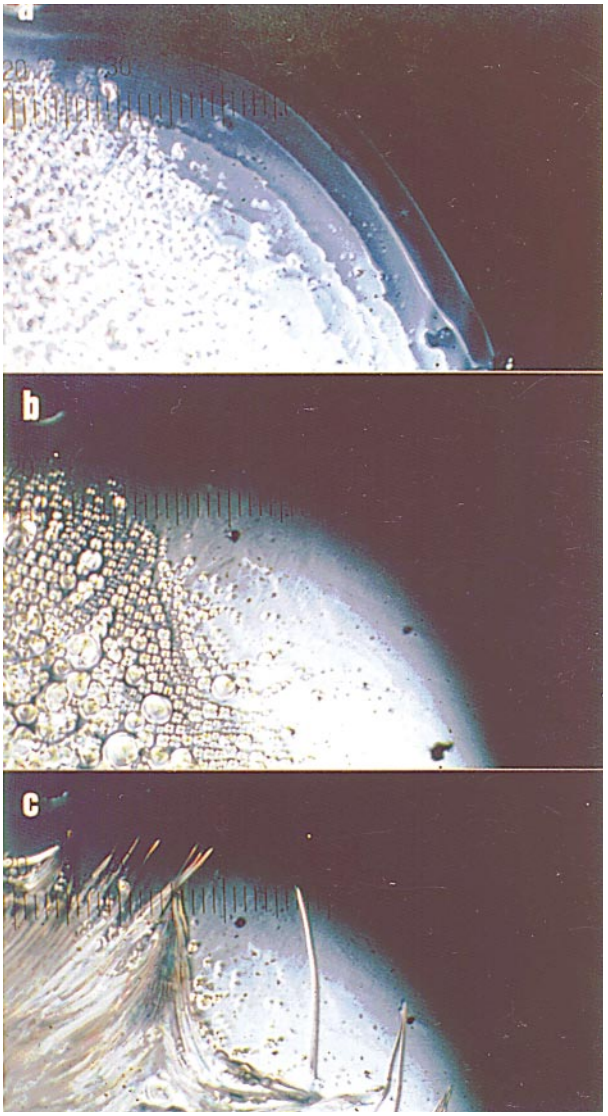

Fig. 5 Typical textures of an uncovered droplet of **S1B6**: (a) SmC* phase, (b) SmA* phase and (c) filament texture of the TGB_A* state; ten units of scale = 70 μm

0.839. With x_{3SS} being the molar fraction of **3*SS*** in the binary mixture of diastereomers **3*SS*/3*SR***, integration of the isolated doublet between δ 0.815 and 0.88 gives a proton intensity of $3x_{3SS} = 2.356$ and integration of the rest between δ 0.72 and 0.815 equals $6x_{3SR} + 3x_{3SS} = 3.644$ and consequently $3x_{3SR} = 0.215$ which leads to an ee of 57%.

A binary mixture of diastereomers **3*RS*/3*RR*** shows the ^1H NMR spectrum depicted in Fig. 9 (lower curve). By analogy, an absolute ee = 63% is deduced from $x_{3RS} = 0.814$ and $3x_{3RR} = 0.186$. The differences in the two ee values are within experimental error, which underlines that chiral differentiation of the alcohol derivatives is negligible. Therefore, the average ee of compound **1** amounts to 60%. Since the same path of esterification (*cf.* Synthesis section) affords ferroelectric liquid crystals **S1B*n***, their ee is assumed to be 60%. Due to the linear dependence between the spontaneous polarization P_s and ee,[27] values of optically pure **S1B*n*** are extrapolated and depicted in Fig. 10.

Spontaneous polarization and tilt angle measurement

Fig. 11 depicts typical textures of compound **S1B8** prepared in a 4 μm thick LC cell. A 'striped bookshelf structure' with equidistant lines approximately equal to the cell thickness is shown in Fig. 11(*a*). A ferroelectric domain structure is formed on cooling the cell into the SmC* phase [*cf.* Fig. 11(*b*)] without

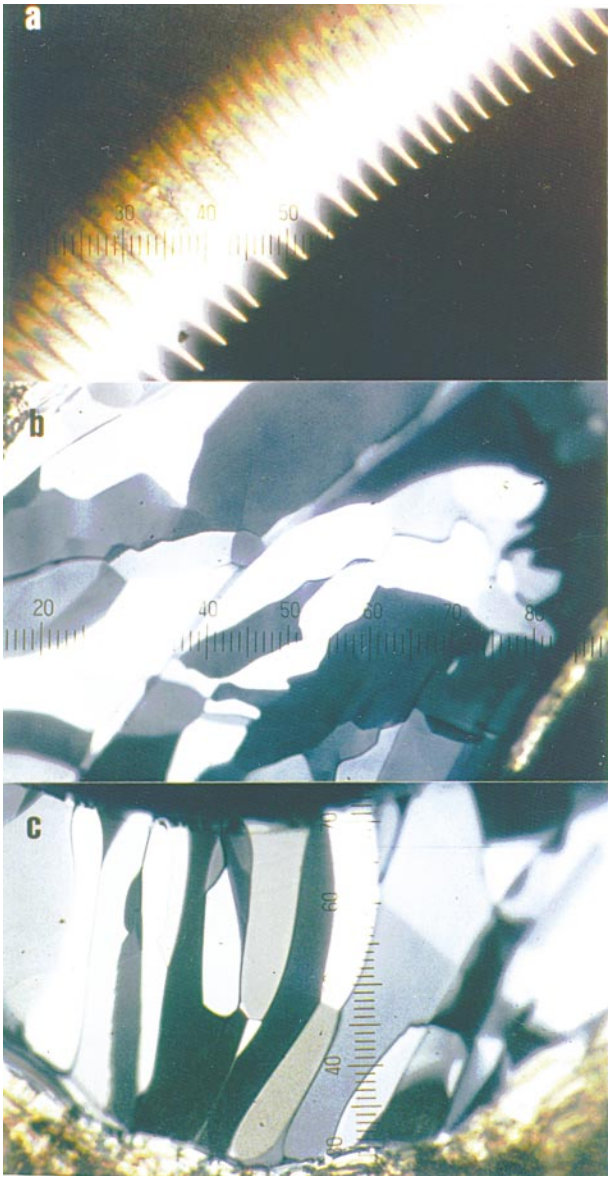

Fig. 6 Typical textures of a free standing film of **S1B6**: (a) filament texture of the TGB_A* state, (b) platelet texture of the SmX_1* phase (c) texture of SmX_2* phase; ten units of scale = 70 μm

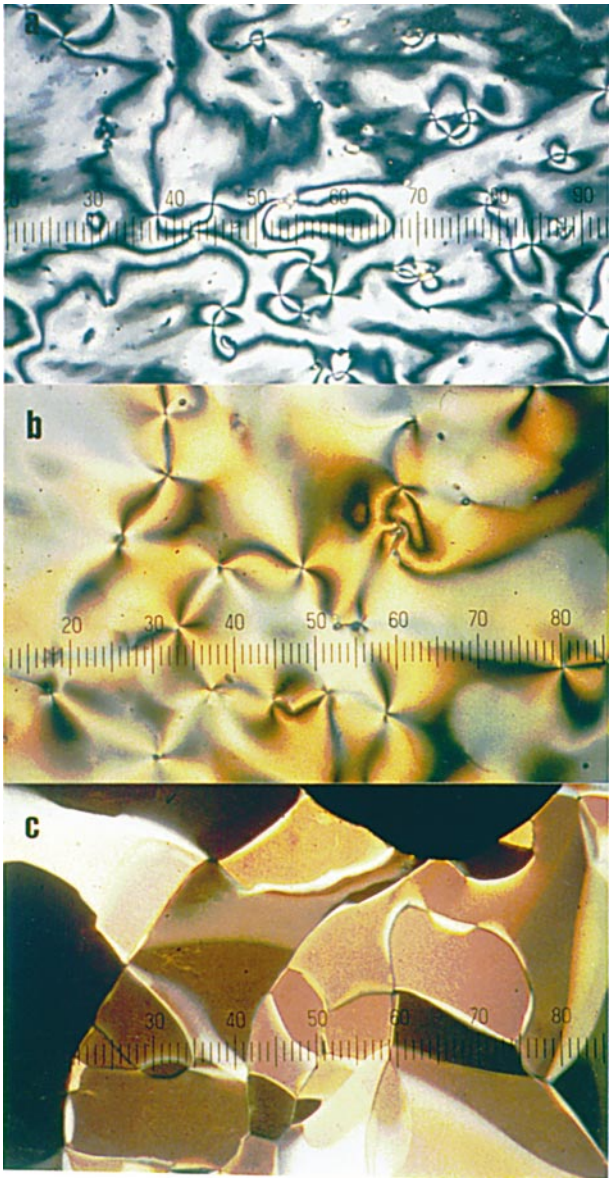

Fig. 7 Typical textures of homeotropic aligned smectic phases of compound **S1B7**: (a) Schlieren texture of the SmC* phase, (b) Schlieren texture of the SmX_1* phase, (c) texture of SmX_2* phase; ten units of scale = 70 μm

any electric field applied. This nearly bookshelf like spatial director configuration is transformed into a 'horizontal chevron structure' after application of a large (20 MV m^{-1}) bias electric field,[28] which causes a movement of smectic layers to form two types of domains with their smectic layer normal oriented parallel to the substrate and inclined at an angle of 2Θ [*cf.* Fig. 11(*c*)]. Measurements of the spontaneous polarization are performed in cells with a 'horizontal chevron structure' present. The optical tilt angle is determined in an area of one type of the domains depicted in Fig. 11(*c*).

Fig. 12 represents the spontaneous polarization P_s measured in the SmC* phase of homologues with $3 \leqslant n \leqslant 7$ as a function of reduced temperature $T - T_c$ in the vicinity of the SmA*→SmC* phase transition (T_c). After passing the SmA*→SmC* phase transition on cooling, the spontaneous polarization rises continuously, less pronounced with increasing molecular length n, as does P_s. This might be related to a decreasing number of chiral dipoles within a unit volume due to the insertion of methylene groups. Far below the SmA*→SmC* phase transition, a linear increase of P_s is established in contrast to the behavior of the optical tilt angle Θ_{opt} as well as the tilt angle determined from the smectic layer thickness $\Theta_{X\text{-}ray}$ depicted in Fig. 13 together with the spontaneous polarization. In the low temperature range of the SmC* phase, this behavior is related to a non-linear coupling between tilt and spontaneous polarization.

In agreement with results by various authors for several compounds,[29,30] the evolution of $\Theta_{opt}(T)$ and $\Theta_{X\text{-}ray}(T)$ differs remarkably. As deduced from Fig. 13–15, the optical tilt angle $\Theta_{opt}(T)$ rises in a less pronounced way in comparison to $\Theta_{X\text{-}ray}(T)$ and both curves intersect a few degrees below the phase transition temperature.[31] In the vicinity of the SmA*→SmC* phase transition, the electroclinic effect alters the value of Θ_{opt} in comparison to values measured at zero electric field or in a racemic mixture.

Quadrupolar coupling

According to the classical Landau model, the free enthalpy density g is expanded in an even power series of the primary order parameter Θ in the vicinity of a SmA→SmC phase transition. The series is truncated after the third term. The first Landau coefficient $a = \alpha(T - T_c)$ changes sign at the phase transition temperature T_c [eqn. (1)].

$$g = g_0 + \alpha(T - T_c)\Theta^2 + b\Theta^4 + c\Theta^6 \quad (1)$$

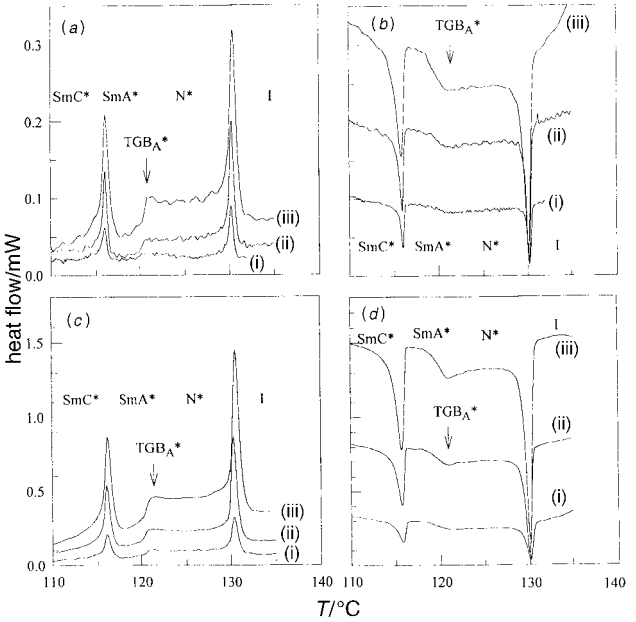

Fig. 8 DSC traces of compound **S1B6** obtained in the vicinity of the TGB_A* phase as a function of the sample mass and the heating–cooling rate: (*a*) sample mass: 0.92 mg, heating rates: (i) +2, (ii) +5, (iii) +10 K min^{-1}; (*b*) cooling: sample mass: 0.92 mg, cooling rates: (i) −2, (ii) −5, (iii) −10 K min^{-1}; (*c*) heating rate: +10 K min^{-1}, sample masses: (i) 0.92, (ii) 2.25, (iii) 3.99 mg; (*d*) cooling rate: −10 K min^{-1}, sample masses: (i) 0.92, (ii) 2.25, (iii) 3.99 mg

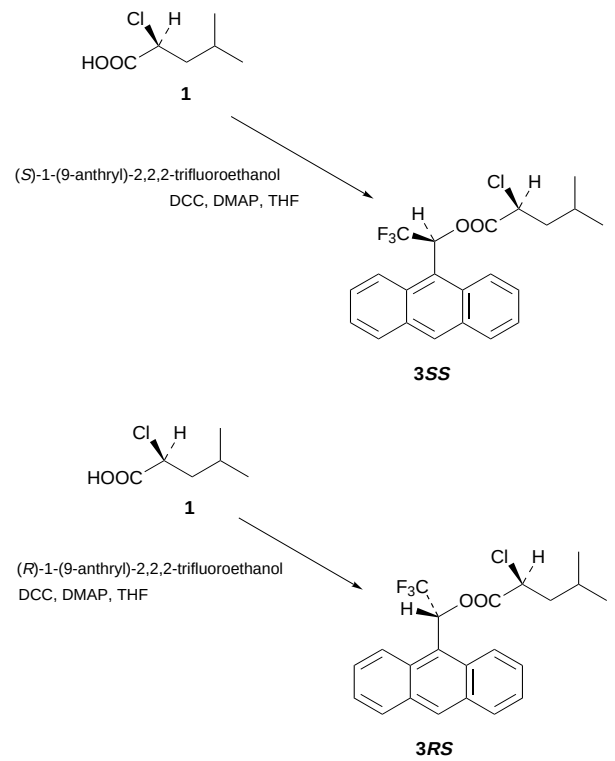

Scheme 2 Synthesis of diastereomers

In a uniformly oriented LC material in the surface stabilized geometry without elastic deformations of the spatial director configuration, a flexoelectric polarization is non-existent. Within an electric field E the electrostatic term $P^2/2\chi$ is added to g, where χ denotes the static dielectric susceptibility measured along the direction of the electric field. Considering chiral material, the bilinear coupling between the tilt angle Θ and the secondary order parameter P includes a spontaneous part P_s of the total electric polarization P. In the absence of

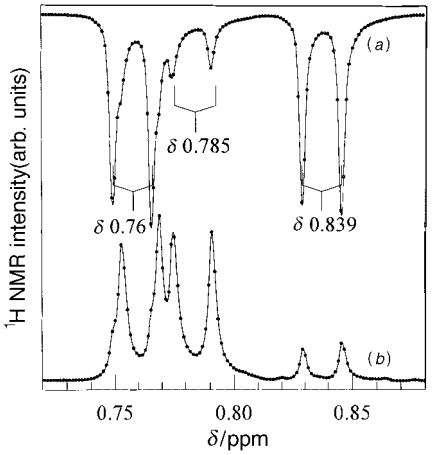

Fig. 9 ^{1}H NMR (400 MHz, $CDCl_3$) spectra of mixtures of diastereomers in the methyl (CH_3) absorption range; the upper spectrum is represented as a mirror image at the abscissa, *e.g.* esterification of (*S*)-1-(9-anthryl)-2,2,2-trifluoroethanol with (*S*)-2-chloro-4-methylpentanoic acid affords compound **3*SS***, whose methyl protons give well separated doublets located at $\delta = 0.76$ and $\delta = 0.839$. Compound **3*SR***, which is formed by esterification of (*S*)-1-(9-anthryl)-2,2,2-trifluoroethanol and (*R*)-2-chloro-4-methylpentanoic acid, shows two doublets located at $\delta = 0.785$ and $\delta = 0.76$ (shoulder) [spectrum (*a*); **3*SS***:**3*SR*** = 8:2]. The diastereoisomeric excess is derived from integration of these spectra as described in the text. By analogy, (*R*)-1-(9-anthryl)-2,2,2-trifluoroethanol affords compounds **3*RS*** and **3*RR*** [spectrum (*b*); **3*RS***:**3*RR*** = 8:2].

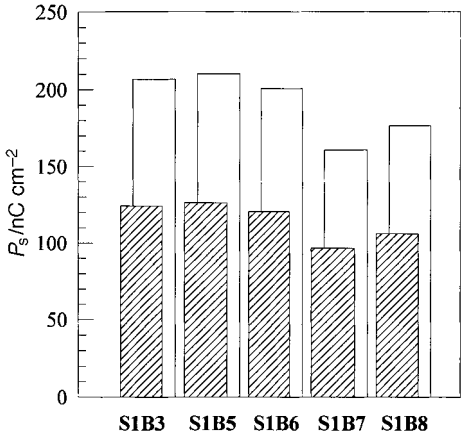

Fig. 10 Extrapolation of the spontaneous polarization of **S1B*n*** due to the influence of the enantiomeric excess

an electric field, P equals P_s. The piezoelectric constant C describes the bilinear coupling and the chiral term $-C\Theta P$ is also added to g.

Following the ideas proposed by Žekš and Blinc, usually referred to as the 'generalized Landau model', an achiral biquadratic coupling term $-\Omega P^2\Theta^2/2$ due to transverse quadrupolar ordering is added to the free energy density g [eqn. (2)].

$$g = g_0 + \alpha(T - T_c)\Theta^2 + b\Theta^4 + c\Theta^6 + \frac{P^2}{2\chi} - C\Theta P - \tfrac{1}{2}\Omega P^2\Theta^2. \qquad (2)$$

Originally, a biquadratic polarization term $\eta P^4/4$ was also added for stability reasons. A physical meaning has yet to be found. Our experimental data can be fitted to eqn. (2), and therefore, the η-term is omitted in the following approach. By minimization of eqn. (2) with respect to the total polarization P, the polarization tilt coupling reads as in eqn. (3).

$$P = \frac{\chi C\Theta}{1 - \chi\Omega\Theta^2} \qquad (3)$$

Here, the total polarization P, the tilt angle Θ and the susceptibility χ can be measured as a function of temperature

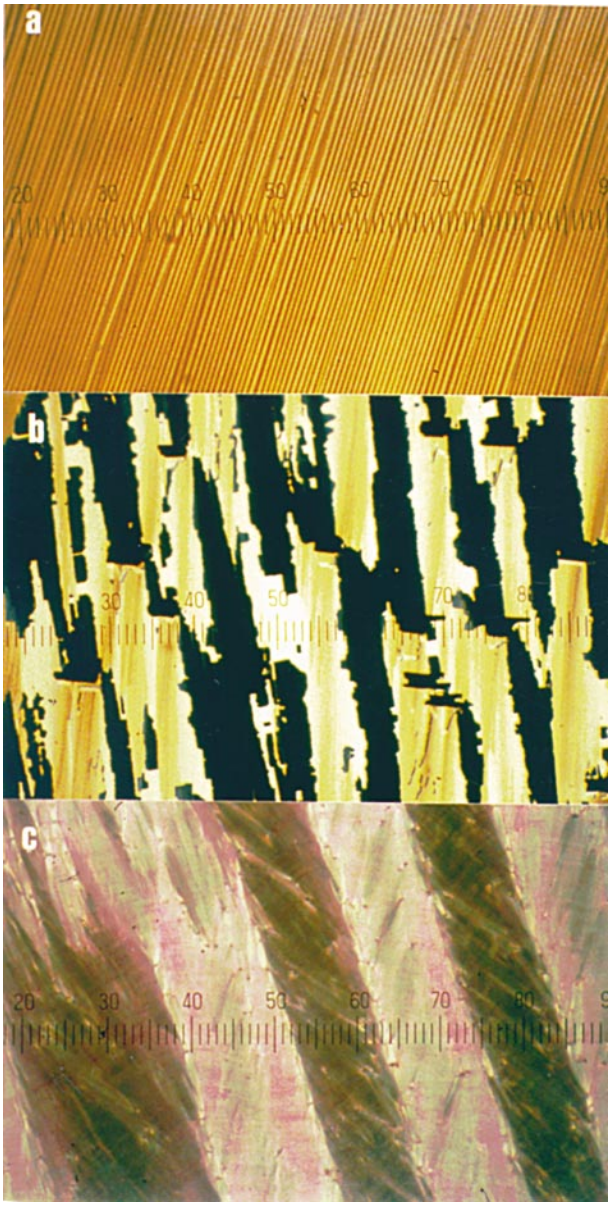

Fig. 11 Typical textures of compound **S1B8** being prepared in a 4 μm thick LC cell: (a) striped bookshelf structure of the SmA* phase, (b) ferroelectric domain structure of the SmC* phase, (c) horizontal chevron structure of the SmC* phase; ten units of scale = 70 μm

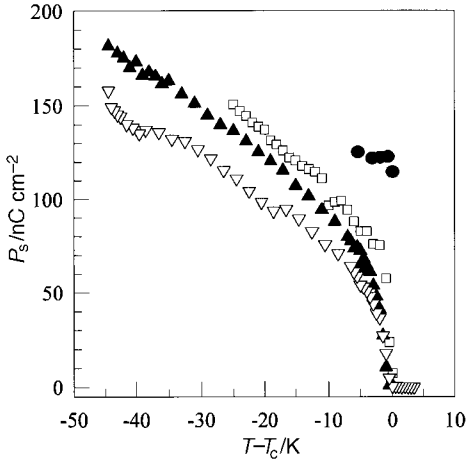

Fig. 12 Temperature dependence of the spontaneous polarization of the homologous series **S1B*n***; (●) $n=3$; (□) $n=5$; (▲) $n=6$; (▽) $n=7$

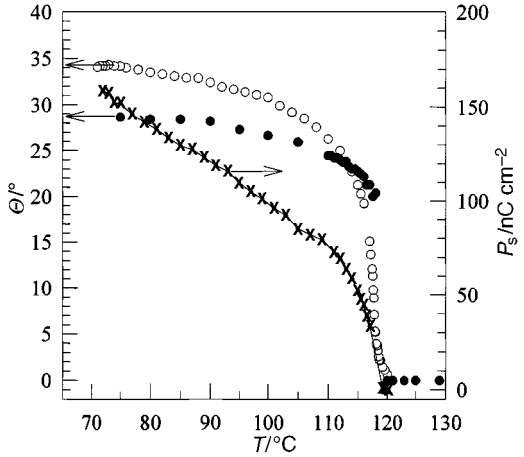

Fig. 13 Spontaneous polarization (×) versus temperature in comparison the optical tilt angle (○) and the tilt angle determined from measurements of the smectic interlayer spacing (●) for **S1B8**

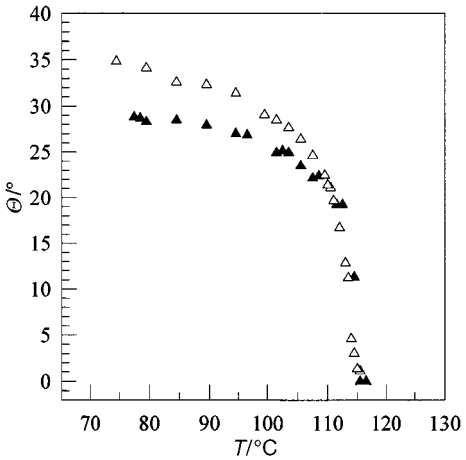

Fig. 14 Comparison between the optical tilt angle (▲) and the tilt angle determined from measurements of the smectic interlayer spacing (△) for **S1B6**

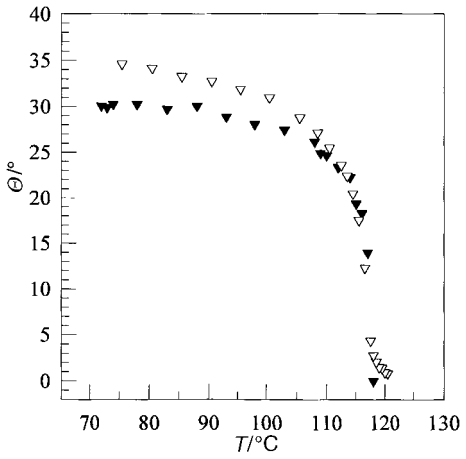

Fig. 15 Comparison between the optical tilt angle (▼) and the tilt angle determined from measurements of the smectic interlayer spacing (▽) for **S1B7**

and the piezoelectric coupling constant C and the quadrupolar coupling constant Ω are determined by fitting eqn. (3) to experimental data.[32] Far below the SmA*→SmC* phase transition, the electroclinic effect is negligible and the dielectric part of the total polarization can be neglected in comparison to the spontaneous polarization P_s, even if an electric field is applied for measurement of the polarization and the optical tilt angle.

In this temperature range the approximation $P \simeq P_s$ holds and deviations from a linear tilt angle to polarization coupling arises from quadrupolar ordering. In Fig. 16–18, the spontaneous polarization is plotted *versus* optical tilt angles and tilt angles derived from X-ray scattering, respectively. The solid lines denote best fits according to eqn. (3). In general, quadrupolar coupling constants Ω are larger for P_s being fitted to $\Theta_{X\text{-ray}}$ in comparison to P_s being fitted to Θ_{opt} as can be inferred from the tilt and polarization measurements in homologues **S1B*n*** with $6 \leqslant n \leqslant 8$.

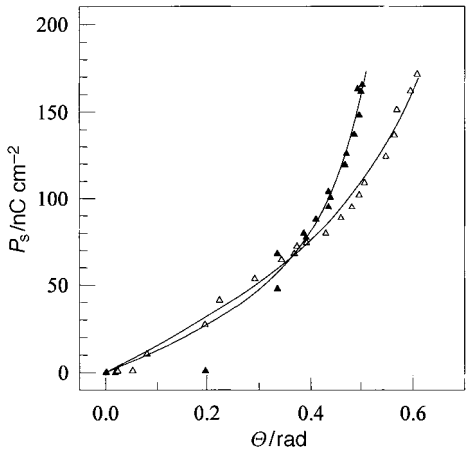

Fig. 16 Tilt angle to polarization coupling for compound **S1B6** from optical (▲) and X-ray (△) measurements

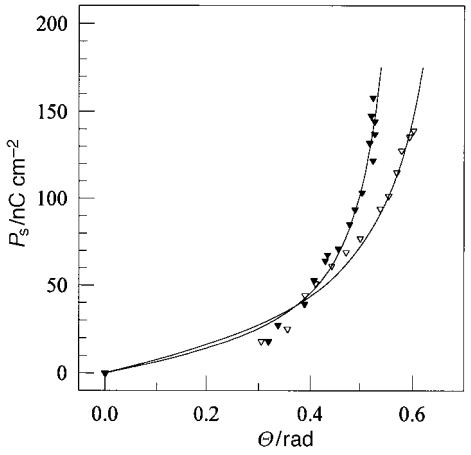

Fig. 17 Tilt angle to polarization coupling for compound **S1B7** from optical (▼) and X-ray (▽) measurements

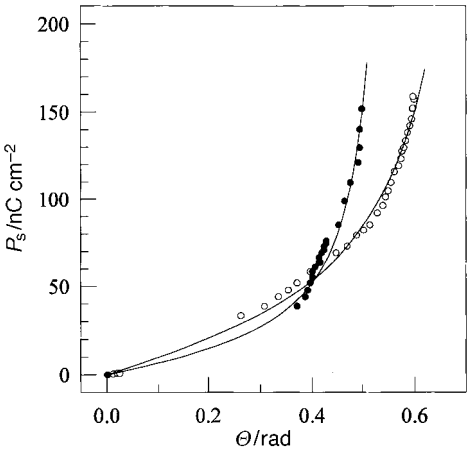

Fig. 18 Tilt angle to polarization coupling for compound **S1B8** from optical (○) and X-ray (●) measurements

Summary

The homologous series **S1B*n*** derived from L-leucine have been synthesized and characterized with respect to their mesomorphic and chiral properties. Elongation of the molecules suppresses crystallization and leads to formation of enantiotropic liquid crystalline phases with the phase sequence: N*, SmC*, SmA*, SmX_1*. Compound **S1B6** undergoes a transition from N* to SmA* phase *via* an intermediate TGB_A* state. The TGB_A* state is suppressed by surface interactions in thin cells or freely suspended films. DSC measurements show a continuous phase transition connected to a change of $|\Delta\overline{c_p}| = 135$ J $K^{-1}mol^{-1}$, whereas the SmA*→SmC* phase transitions appear to be first order like. Using the same method of esterification, diastereoisomeric compounds have been synthesized, which allow the determination of the ee value as 60% by ^{1}H NMR spectroscopy. Linear extrapolation of the spontaneous polarization to the pure enantiomers leads to values in the range of those obtained for other α-chloro acid derivatives.[3–11]

Tilt angles calculated from smectic layer spacings measured by X-ray scattering and tilt angles obtained from ferroelectric switching being recorded in optical transmission signals differ remarkably even in a temperature range far below the SmA*→SmC* phase transition. Data sets are successfully fitted to the 'generalized Landau model' proposed by Žekš and Blinc.

Conclusion

Optical measurements and X-ray investigations yield different values of 'tilt angles' which are related to each other.[33] Both can be discussed in the framework of the 'generalized Landau model' to derive the bilinear and quadrupolar coupling between a 'tilt angle' and the electric polarization and the resulting bilinear and quadrupolar coupling coefficient depending on the measurement technique, respectively.

Besides this concept, the 'tilt direction' and the 'tilt angle Θ' are still 'ill defined' since[34] both the non-chiral SmC and the chiral SmC* are biaxial; therefore, this one parameter concept may lead to Θ values depending on measurement technique. The direction of the largest eigenvalue of *e.g.* its dielectric tensor at some specified frequency can be used to define a 'tilt angle' more precisely. The whole concept of a 'tilt angle' used as primary order parameter in the 'generalized Landau model' has to be set on firm ground and a precise evaluation of its coefficients requires a precise measurement of Θ.

Synthesis

The following compounds were received from Aldrich-Sigma GmbH and used without further purification: 4-alkylbenzoic acids, L-leucine, 4,4′-dihydroxybiphenyl, (*R*)- and (*S*)-1-(9-anthryl)-2,2,2-trifluoroethanol, dicyclohexylcarbodiimide (DCC) and 4-(dimethylamino)pyridine (DMAP). Liquid chromatography was carried out on silica gel 60 (Merck, 0.063–0.200 mm) with dichloromethane as eluent. Tetrahydrofuran (THF) was dried over sodium, distilled and used immediately.

(*S*)-2-Chloro-4-methylpentanoic acid 1

L-Leucine (0.2 mol, 25 g) was dissolved in a mixture of 550 cm^3 of 37% HCl and 260 cm^3 of water at room temperature. The solution was cooled to −3 °C. During a period of 5 h, 0.32 mol (22 g) of solid $NaNO_2$ was added in small portions under vigorous stirring. The solution turned yellow and phase separation between the crude product and the inorganic layer occurred. Stirring was continued for another 4 h and the temperature was allowed to increase to room temperature. The solution was quenched with 1200 cm^3 of ice–water mixture and extracted with diethyl ether (3×300 cm^3). The combined

organic extracts were washed with 10% $NaHCO_3$ solution ($2\times100\ cm^3$) and water ($2\times100\ cm^3$) and dried over anhydrous $MgSO_4$. The solvent was evaporated and the crude product was distilled under reduced pressure to afford 18 g of **1**, yield 18 g (60%); bp 109 °C, 10 mmHg [lit.,[35,36] bp 110–112 °C at 10 mmHg; however, we find partial racemisation, which leads to the ee measured in this work (60%), which is much smaller than the value (95.8%) reported by Koppenhofer *et al.* Different reaction conditions may cause the difference.]; $n_D^{25}=1.4441$; δ_H ($CDCl_3$, 400 MHz; *J* values in Hz throughout): 0.94 (3H, d, *J* 6.1, CH_3), 0.98 (3H, d, *J* 6.1, CH_3), 1.05 [1H, m, CH(CH_3)$_2$], 1.87 [2H, m, HCH–CH(CH_3)$_2$], 4.35 [1H, m, CH(Cl)], 8.8 (1H, br, COOH); $^{13}C\{^1H\}$ δ_C ($CDCl_3$, 100 MHz): 21.0 (CH_3), 22.6 (CH_3), 25.1 [CH(CH_3)$_2$], 43.3 (CH_2), 55.6 [CH(Cl)], 175.9 (COOH); *m/z* 150, 152 (M^+, 10%), 133 (9), 94 (32), 73 (48), 69 (75), 57 (70), 43 (100), 39 (45).

4-[(*S*)-2-Chloro-4-methylpentanoyloxy]-4′-hydroxybiphenyl 2

Two pathways for esterification of **1** were used to give **2**: (*i*) *via* acid chloride and (*ii*) with the help of the DCC–DMAP system. The ee did not depend on the method of esterification in contrast to results reported in literature.[9]

(*i*) The acid **1** (14 mmol, 2 g) was mixed with 10 cm^3 of $SOCl_2$ under a dry nitrogen atmosphere. The solution was kept for a week in a refrigerator at 5 °C until evolution of HCl gas had stopped. Dry benzene (3 cm^3) was added and the excess of $SOCl_2$ (together with benzene) was removed under reduced pressure with the temperature kept below 30 °C. The oily residue was dissolved in dry $CHCl_3$ and used without further purification.

4,4′-Dihydroxybiphenyl (27 mmol, 5 g) was dissolved in a mixture of 5 cm^3 of pyridine and 15 cm^3 of dry $CHCl_3$ and the solution was cooled to 3 °C in an ice bath. The solution of the acid chloride in $CHCl_3$ previously prepared was added dropwise *via* a syringe under vigorous stirring. The reaction mixture was stirred for 2 h and the temperature was allowed to increase to room temperature. The reaction mixture was poured into a solution of 10 cm^3 of concentrated hydrochloric acid in 400 cm^3 of water, esters were extracted into $CHCl_3$ ($3\times50\ cm^3$) and the precipitate (excess of 4,4′-dihydroxybiphenyl) was filtered off and extracted with 50 cm^3 of boiling $CHCl_3$. The combined $CHCl_3$ extracts were washed with 10% $NaHCO_3$ solution ($2\times50\ cm^3$) and water ($2\times50\ cm^3$) and dried over anhydrous Na_2SO_4. $CHCl_3$ was evaporated and the crude product was subjected to column chromatography (eluent CH_2Cl_2). The second product was collected ($R_f=0.35$) and after evaporation of CH_2Cl_2 the crude product was recrystallized twice from absolute EtOH and cyclohexane to afford 1.12 g of pure **2** as a white powder, yield 25%.

(*ii*) 4,4′-Dihydroxybiphenyl (27 mmol, 5 g) was dissolved in 100 cm^3 of dry THF and a solution of 14 mmol (2 g) of **1** in 10 cm^3 of dry THF was added dropwise under vigorous stirring at room temp. Simultaneously, a mixture of 3.1 g (15 mmol) of DCC and 10 mg of DMAP in 10 cm^3 of dry THF was added dropwise. After 10 min a white precipitate appeared. The reaction mixture was stirred overnight and the precipitate was filtered off and washed with 10 cm^3 of THF. The THF extracts were collected and the solvent was evaporated under reduced pressure. The crude white product was dissolved in CH_2Cl_2 washed with water ($2\times50\ cm^3$) and dried over anhydrous Na_2SO_4. CH_2Cl_2 was evaporated and the residue was purified by column chromatography (eluent CH_2Cl_2). Further purification was performed by analogy to (*i*) and afford 1.38 g of pure **2**, yield 31%.

Mp 123 °C, δ_H ($CDCl_3$, 400 MHz): 1.00 (3H, d, *J* 6.0, CH_3), 1.04 (3H, d, *J* 6.0, CH_3), 1.90–1.99 (1H, m), 1.98–2.04 (2H, m), 4.56 [1H, dd, *J* 7.6, CH(Cl)], 5.4 (1H, br, OH), 6.85 (2H, d, *J* 8.6), 7.15 (2H, d, *J* 8.6), 7.40 (2H, d, *J* 8.6), 7.52 (2H, d, *J* 8.6); $^{13}C\{^1H\}$ δ_C ($CDCl_3$, 100 MHz): 21.5 (CH_3), 22.6 (CH_3), 25.3 [CH(CH_3)$_2$], 43.4 (CH_2), 55.7 [CH(Cl)], 115.7, 121.3, 127.8, 128.3 (*C*H arom.), 132.7, 139.1, 149.2, 155.3 (*C* arom.), 168.0 [H(Cl)C—*C*OO]; *m/z* 318, 320 (M^+, 27%), 186 (100), 157 (10), 128 (6), 102 (1), 97 (2), 77 (5), 69 (6), 55 (6), 43 (7).

4-[(*S*)-2-Chloro-4-methylpentanoyloxy]-4′-[4-alkylbenzoyloxy]biphenyl (S1B*n*)

The biphenyl derivative **2** (2 mmol, 0.64 g) and 2.2 mmol of 4-*n*-alkylbenzoic acid were dissolved in 10 cm^3 of dry THF. 2.4 mmol (0.5 g) of DCC and 0.04 mmol (5 mg) of DMAP were added, and the reaction mixture was stirred overnight at room temperature. The white precipitate was filtered off, washed with 2 cm^3 of THF, and the THF was evaporated under reduced pressure. The crude white product was subjected to column chromatography (CH_2Cl_2–hexane, 9:1, v/v as eluent). The product was collected, the solvent evaporated, and the white powder recrystallized from absolute EtOH. Column chromatography and recrystallization were repeated once to afford pure liquid crystals **S1B*n*** ($n=2$–8) with a sufficiently low ionic conductivity.

S1B2: yield 0.39 g, 43% δ_H ($CDCl_3$, 400 MHz): 1.02 [6H, dd, CH(CH_3)$_2$], 1.29 (3H, t, CH_2CH_3), 2.00 [3H, m, CH_2CH(CH_3)$_2$], 2.76 (2H, q, C$H_2$$CH_3$), 4.52 [1H, dd, C$H$(Cl)], 7.29 (6H, m), 7.61 (4H, d), 8.15 (2H, d); $^{13}C\{^1H\}$ δ_C ($CDCl_3$, 100 MHz): 15.3 (CH_2—CH_3), 21.5, 22.6 [CH(CH_3)$_2$], 25.3 [CH(CH_3)$_2$], 43.4 [CH_2CH(Cl)], 55.7 [CH(Cl)], 121.5–150.7 (*C* arom.), 165.3 (Ph*C*OOPh), 168.6 [H(Cl)C—*C*OO]; *m/z* 450, 452 (M^+, 6%), 435 (0.1), 415 (0.1), 399 (0.1), 371 (0.1), 318 (1), 185 (3), 157 (2), 133 (100), 105 (9), 79 (10), 55 (2), 43 (6)

S1B3: yield 0.37 g, 40% δ_H ($CDCl_3$, 400 MHz): 0.97 [3H, t, (CH_2)$_2$CH_3] 1.02 [6H, dd, CH(CH_3)$_2$], 1.70 (2H, m, CH_2C$H_2$$CH_3$), 2.01 [3H, m, C$H_2CH$($CH_3$)$_2$], 2.69 (2H, t, C$H_2$$CH_2$$CH_3$), 4.55 [1H, dd, C$H$(Cl)], 7.27 (6H, m), 7.61 (4H, d), 8.45 (2H, d); $^{13}C\{^1H\}$ δ_C ($CDCl_3$, 100 MHz): 13.8 [(CH_2)$_2$CH_3], 21.5, 22.6 [CH(CH_3)$_2$], 24.3 (CH_2C$H_2$$CH_3$), 25.3 [$CH$($CH_3$)$_2$], 38.1 ($CH_2$$CH_2$$CH_3$), 43.4 [$CH_2$CH(Cl)], 55.7 [$CH$(Cl)], 121.5–150.6 (*C* arom.), 165.3 (Ph*C*OOPh), 168.6 [H(Cl)C—*C*OO]; *m/z* 464, 466 (M^+, 5%), 449 (0.2), 429 (0.1), 413 (0.1), 385 (0.1), 332 (1), 185 (4), 157 (2), 147 (100), 131 (1), 119 (5), 103 (2), 91 (15), 69 (6), 51 (5), 43 (7), 32 (5)

S1B5: yield 0.32 g, 32%; δ_H ($CDCl_3$, 400 MHz): 0.91 [3H, t, (CH_2)$_4$CH_3] 1.02 [6H, dd, CH(CH_3)$_2$], 1.35 [4H, m, CH_2(CH_2)$_2$$CH_2$$CH_3$], 1.66 [2H, m, CH_2(CH_2)$_2$C$H_2$$CH_3$], 1.97 [3H, m, C$H_2CH$($CH_3$)$_2$], 2.71 [2H, t, C$H_2$($CH_2$)$_3$$CH_3$], 4.56 [1H, dd, C$H$(Cl)], 7.27 (6H, m), 7.61 (4H, d), 8.13 (2H, d); $^{13}C\{^1H\}$ δ_C ($CDCl_3$, 100 MHz): 14.02 [(CH_2)$_4$CH_3], 21.5, 22.6 [CH(CH_3)$_2$], 22.5 (CH_3C$H_2$$CH_3$), 25.3 [$CH$($CH_3$)$_2$], 30.8 ($CH_2$$CH_2$$CH_3$), 31.4 [$CH_2$($CH_2$)$_2$$CH_3$], 36.1 [$CH_2$($CH_2$)$_3$$CH_3$], 43.4 [$CH_2$CH(Cl)], 55.7 [$CH$(Cl)], 121.5–150.6 (*C* arom.), 165.3 (Ph*C*OOPh), 168.6 [H(Cl)C—*C*OO]; *m/z* 492, 494 (M^+, 3%), 477 (0.3), 459 (0.1), 441 (0.7), 413 (0.4), 360 (1.5), 185 (3), 175 (100), 157 (2), 131 (2), 118 (2.5), 105 (1), 91 (20), 69 (8), 51 (9), 43 (10), 32 (10)

S1B6: yield 0.35 g, 35%; δ_H ($CDCl_3$, 400 MHz): 0.89 [3H, t, (CH_2)$_5$CH_3] 1.02 [6H, dd, CH(CH_3)$_2$], 1.33 [6H, m, CH_2(CH_2)$_3$$CH_2$$CH_3$], 1.65 [2H, m, CH_2(CH_2)$_3$C$H_2$$CH_3$], 1.98 [3H, m, C$H_2CH$($CH_3$)$_2$], 2.71 [2H, t, C$H_2$($CH_2$)$_4$$CH_3$], 4.56 [1H, dd, C$H$(Cl)], 7.27 (6H, m), 7.61 (4H, d), 8.13 (2H, d); $^{13}C\{^1H\}$ δ_C ($CDCl_3$, 100 MHz): 14.09 [(CH_2)$_5$CH_3], 21.5, 22.6 [CH(CH_3)$_2$], 22.6 (CH_3C$H_2$$CH_3$), 25.3 [$CH$($CH_3$)$_2$], 28.9 ($CH_2$$CH_2$$CH_3$), 31.1 [$CH_2$($CH_2$)$_2$$CH_3$], 31.7 [$CH_2$($CH_2$)$_3$$CH_3$], 36.1 [$CH_2$($CH_2$)$_4$$CH_3$], 43.4 [$CH_2$CH(Cl)], 55.7 [$CH$(Cl)], 121.5–150.6 (*C* arom.), 165.3 (Ph*C*OOPh), 168.6 [H(Cl)C—*C*OO]; *m/z* 506, 508 (M^+, 2%), 491 (0.3), 473 (0.1), 455 (0.8), 427 (0.3), 373 (1), 189 (100), 185 (4), 157 (2), 131 (2), 118 (2.5), 105 (1), 91 (18), 69 (7), 51 (7), 43 (9), 32 (9)

S1B7: yield 0.45 g, 40%; δ_H ($CDCl_3$, 400 MHz): 0.88 [3H, t,

$(CH_2)_5CH_3$], 1.02 [6H, dd, $CH(CH_3)_2$], 1.30 [8H, m, $CH_2(CH_2)_3CH_2CH_3$], 1.66 [2H, m, $CH_2(CH_2)_3CH_2CH_3$], 1.98 [3H, m, $CH_2CH(CH_3)_2$], 2.71 [2H, t, $CH_2(CH_2)_4CH_3$], 4.55 [1H, dd, CH(Cl)], 7.27 (6H, m), 7.60 (4H, d), 8.14 (2H, d); $^{13}C\{^1H\}$ δ_C ($CDCl_3$, 100 MHz): 14.21 [$(CH_2)_5CH_3$], 21.5, 22.6 [$CH(CH_3)_2$], 22.5 [$CH_3CH_2CH_3$], 25.3 [$CH(CH_3)_2$], 29.9 ($CH_2CH_2CH_3$), 31.3 [$CH_2(CH_2)_2CH_3$], 31.8 [$CH_2(CH_2)_3CH_3$], 36.0 [$CH_2(CH_2)_4CH_3$], 40.0 [$CH_2(CH_2)_5CH_3$], 43.4 [$CH_2CH(Cl)$], 55.7 [CH(Cl)], 121.5–150.6 (*C* arom.), 165.3 (Ph*C*OOPh), 168.7 [H(Cl)C—*C*OO]; *m/z* 520, 522 (M^+, 2%), 505 (0.5), 487 (0.2), 449 (1), 441 (0.5), 388 (2), 203 (100), 185 (3), 157 (1), 131 (2), 118 (2.5), 105 (2), 91 (18), 69 (9), 51 (9), 43 (12), 32 (9)

S1B8: yield 0.40 g, 31% δ_H ($CDCl_3$, 400 MHz): 0.89 [3H, t, $(CH_2)_5CH_3$], 1.01 [6H, dd, $CH(CH_3)_2$], 1.29 [8H, m, $CH_2(CH_2)_3CH_2CH_3$], 1.64 [2H, m, $CH_2(CH_2)_3CH_2CH_3$], 2.00 [3H, m, $CH_2CH(CH_3)_2$], 2.71 [2H, t, $CH_2(CH_2)_4CH_3$], 4.54 [1H, dd, CH(Cl)], 7.29 (8H, m), 7.60 (4H, d), 8.14 (2H, d); $^{13}C\{^1H\}$ δ_C ($CDCl_3$, 100 MHz): 15.80 [$(CH_2)_5CH_3$], 21.4, 22.5 [$CH(CH_3)_2$], 22.4 ($CH_3CH_2CH_3$), 25.1 [$CH(CH_3)_2$], 29.7 ($CH_2CH_2CH_3$), 31.2 [$CH_2(CH_2)_2CH_3$], 31.7 [$CH_2(CH_2)_3CH_3$], 36.1 [$CH_2(CH_2)_4CH_3$], 39.9 [$CH_2(CH_2)_5CH_3$], 41.1 [$CH_2(CH_2)_6CH_3$], 43.2 [$CH_2CH(Cl)$], 55.5 [CH(Cl)], 121.5–150.7 (*C* arom.), 165.1 (Ph*C*OOPh), 168.5 [H(Cl)C—*C*OO]; *m/z* 534, 536 (M^+, 4%), 519 (1), 501 (1), 483 (1), 455 (2), 402 (3), 217 (100), 185 (6), 157 (3), 131 (4), 118 (5), 105 (3), 91 (17), 69 (10), 51 (8), 43 (7), 32 (7)

(*R*)-1-(9-Anthryl)-1-[(*S*)-2-chloro-4-methylpentanoyloxy]-2,2,2-trifluoroethane (3*RS*)

The acid **1** (0.17 mmol, 26 mg) and 0.15 mmol (41 mg) of (*R*)-1-(9-anthryl)-2,2,2-trifluoroethanol were dissolved in 2 cm^3 of dry THF. 0.2 mmol (41 mg) of DCC and 1 mg of DMAP were added and the reaction mixture was stirred overnight at room temperature. The white precipitate was filtered off. THF was evaporated under reduced pressure, and the crude product purified by column chromatography (CH_2Cl_2 as eluent) to yield 46 mg (66%) of **3*RS*** as a colorless oil, δ_H ($CDCl_3$, 400 MHz): 0.76 [3H, d, *J* 6.6, $CH(CH_3)$], 0.785 [3H, d, *J* 6.6, $CH(CH_3)$], 1.65 (1H, dd, *J* 6.6, $HCHCH(CH_3)_2$], 1.73 [1H, dd, *J* 6.6, $HCH—CH(CH_3)_2$], 1.79 [1H, m, $HCH—CH(CH_3)_2$], 4.38 [1H, dd, *J* 6.6, H(Cl)], 7.38–7.60 (4H, m), 7.74 (1H, m), 7.96 (2H, m), 8.27 (1H, d), 8.50 (1H, s), 8.61 (1H, d); $^{13}C\{^1H\}$ δ_C ($CDCl_3$, 100 MHz): 21.7, 22.8 [$CH(CH_3)_2$], 25.4 [$CH(CH_3)_2$], 43.7 [$CH_2CH(Cl)$], 55.7 [CH(Cl)], 120.6–132.1 (*C* arom.), 168.7 [H(Cl)C—*C*OO]; *m/z* 408, 410 (M^+, 94%), 389 (0.5), 372 (1), 259 (100), 239 (20), 207 (80), 179 (23), 178 (25), 151 (10), 97 (8), 69 (10), 55 (13), 43 (15)

References

1 P. Karrer, H. Reschofsky and W. Kaase, *Helv. Chim. Acta*, 1947, **30**, 271.
2 S. C. J. Fu, S. M. Birnbaum and J. P. Greenstein, *J. Am. Chem. Soc*., 1954, **76**, 6054.
3 T. Sakurai, N. Mikami, R. Higuchi, M. Honma, M. Ozaki and K. Yoshino, *J. Chem. Soc. Chem. Commun*., 1986, 978.
4 Ch. Bahr and G. Heppke, *Mol. Cryst. Liq. Cryst*., 1987, **148**, 29.
5 K. Mohr, S. Köhler, K. Worm, G. Pelzl, S. Diele, H. Zaschke, D. Demus, G. Andersson, I. Dahl, S. T. Lagerwall, K. Skarp and B. Stebler, *Mol. Cryst. Liq. Cryst*., 1987, **146**, 151.
6 K. Yoshino, M. Ozaki, S. Kishio, T. Sakurai, N. Mikami, R. Higuchi and M. Honma, *Mol. Cryst. Liq. Cryst*., 1987, **144**, 87.
7 R. J. Twieg, K. Betterton, H. T. Nguyen, W. Tang and W. Hinsberg, *Ferroelectrics*, 1989, **91**, 243.
8 M. Zgonik, M. Rey-Lafon, C. Destrade, C. Leon and H. T. Nguyen, *J. Phys. (Fr.)*, 1990, **51**, 2015.
9 T. Sierra, J. L. Serrano, M. B. Ros, A. Ezcurra and J. Zubía, *J. Am. Chem. Soc*., 1992, **114**, 7645.
10 I. Dierking, F. Gießelmann, J. Kußerow and P. Zugenmaier, *Liq. Cryst*., 1994, **17**, 243.
11 J. Schacht, I. Dierking, F. Gießelmann, K. Mohr, H. Zaschke, W. Kuczyński and P. Zugenmaier, *Liq. Cryst*., 1995, **19**, 151.
12 S. R. Renn and T. C. Lubensky, *Phys. Rev. A*, 1988, **38**, 2132.
13 O. D. Lavrentovich, Y. A. Nastishin, V. I. Kulishov, Y. S. Narkevich, A. S. Tolochko and S. V. Shiyanowskii, *Europhys. Lett*., 1990, **13**, 313.
14 A. J. Slaney and J. W. Goodby, *Liq. Cryst*., 1991, **9**, 849.
15 L. Navailles, H. T. Nguyen, P. Barois, C. Destrade and N. Isaert, *Liq. Cryst*., 1993, **15**, 479.
16 W. Kuczynski and H. Stegemeyer, *Ber. Bunsenges. Phys. Chem*., 1994, **98**, 1322.
17 J. Schacht, F. Gießelmann and P. Zugenmaier, *Phys. Rev. E*, 1997, **55**, 5633.
18 B. Žekš, *Ferroelectrics*, 1984, **53**, 33.
19 T. Carlsson, B. Žekš, A. Levstik, C. Filipič, I. Levstik and R. Blinc, *Phys. Rev. A*, 1987, **36**, 1484.
20 K. Miyasato, S. Abe, H. Takezoe, A. Fukuda and E. Kuze, *Jpn. J. Appl. Phys*., 1983, **22**, L661.
21 Ch. Bahr and G. Heppke, *Liq. Cryst*., 1987, **2**, 825.
22 H. Baethge, diploma thesis, Clausthal, 1996 (unpublished).
23 R. Cano, *Bull. Soc. fr. Miner. Cristallogr*., 1968, **91**, 20.
24 I. Dierking, F. Gießelmann and P. Zugenmaier, *Liq. Cryst*., 1993, **17**, 17.
25 J. Schacht, F. Gießelmann and P. Zugenmaier, to be published.
26 M. Werth, H. T. Nguyen, C. Destrade and N. Isaert, *Liq. Cryst*., 1994, **17**, 863.
27 Ch. Bahr, G. Heppke and B. Sabaschus, *Ferroelectrics*, 1988, **84**, 103.
28 J. S. Patel, Sin-Doo Lee and J. W. Goodby, *Phys. Rev. A*, 1989, **40**, 2854.
29 S. Kumar, *Phys. Rev. A*, 1981, **23**, 3207.
30 B. I. Ostrovskii, *Soviet Sci. Rev. Sec. A* ed. by I. Khalatnikov, vol. 12, pt. 2, 85.
31 F. Gießelmann and P. Zugenmaier, *Ferroelectrics*, in the press.
32 F. Gießelmann and P. Zugenmaier, *Phys. Rev. E*, 1995, **52**, 1762.
33 F. Gießelmann and P. Zugenmaier, *Phys. Rev. E*, 1997, **55**, 5613.
34 P. G. de Gennes and J. Prost, *The Physics of Liquid Crystals*, 2nd edn., Oxford University Press, Oxford, 1993.
35 A. J. Slaney and J. W. Goodby, *J. Mater. Chem*., 1995, **5**, 663.
36 B. Koppenhoefer and V. Schurig, *Org. Synth*., 1987, **66**, 151.

Paper 7/08126J; *Received* 11*th November*, 1997